Holographic optical tweezers with real-time hologram calculation using a phase-only modulating LCOS-based SLM at 1064 nm

Andreas Hermerschmidt[a], Sven Krüger[a], Tobias Haist[b], Susanne Zwick[b], Michael Warber[b] and Wolfgang Osten[b]

[a] Holoeye Photonics AG, Albert-Einstein-Straße 14, 12489 Berlin, Germany;
[b] Institut für Technische Optik, Universität Stuttgart, Pfaffenwaldring 9, 70569 Stuttgart, Germany

ABSTRACT

We present a method that enables the generation of arbitrary positioned dual-beam traps without additional hardware in a single-beam holographic optical tweezers setup. By this approach stable trapping at low numerical aperture and long working distance is realized with an inverse standard research microscope. Simulations and first experimental results are presented. Additionally we present first steps towards using the method to realize a holographic 4π-microscope. We will also give a detailed analysis of the phase-modulating properties and especially the spatial-frequency dependent diffraction efficiency of holograms reconstructed with the phase-only LCOS spatial light modulator used in our system. Finally, accelerated hologram optimization based on the iterative Fourier transform algorithm is done using the graphics processing unit of a consumer graphics board.

Keywords: holographic tweezers, spatial light modulation, fast hologram computation, graphics processing unit

1. HOLOGRAPHIC TWIN TRAPS

It is well known that microscopic particles can be trapped and moved in the focus of a laser.[1] The light deflected by the particle transfers part of its momentum to the particle. The resulting force can be divided into gradient and scattering force: the gradient force pulls particles with a higher refractive index than the surrounding medium in the direction of highest intensity. The scattering force is directed in the direction of propagation and therefore pushes the particle out of the trap. To achieve stable axial trapping, the gradient force has to exceed the scattering force. In single beam systems this is achieved by employing a microscope objective with high numerical aperture.[1]

Holographic optical tweezers (HOT)[2,3] allow the independent positioning and movement of traps in a simple setup without any mechanical movement. The core element of a HOT setup is the spatial light modulator (SLM) which is positioned in the Fourier plane of the object. A collimated laser illuminates the SLM. The resulting light field behind the SLM is coupled into the microscope (Fig.1). The microscope objective then performs the Fourier transform of the phase-mostly holograms displayed on the SLM. By this approach multiple traps can be dynamically generated and moved independently of each other in all three spatial dimensions with high accuracy. Additionally, different trapping potentials can be generated and aberrations can be corrected.

For our setup an infrared laser (λ=1064 nm, LOT Oriel MOPFA KBS-BTS-YFL-10-PM, 10W, linear polarisation) illuminates the SLM (Holoeye HEO 1080 P II, 1920 $\times$ 1080 pixels, pixel pitch $p = 8\,\mu$m) with a maximum diffraction angle of α =arcsin($\lambda/(2p)$) = 3.81°. The modulated light is coupled into a standard research microscope (Zeiss Axiovert 200M) by imaging the SLM phase-correctly into the entrance pupil of the microscope objective with a magnification of $\beta = 1.8$. The magnification β is a trade-off since the setup is used with different microscope objectives. For further details about the optical design see Haist et al..[4] The holograms are computed on a consumer graphics board using an Nvidia based graphics processing unit (GPU).[5] This setup was used to manipulate beads and cells in all three spatial dimensions. Controlled 3D movement and 3D rotations have been demonstrated.[4]

Further author information: Send correspondence to A.Hermerschmidt, E-mail: andreas.hermerschmidt@holoeye.com

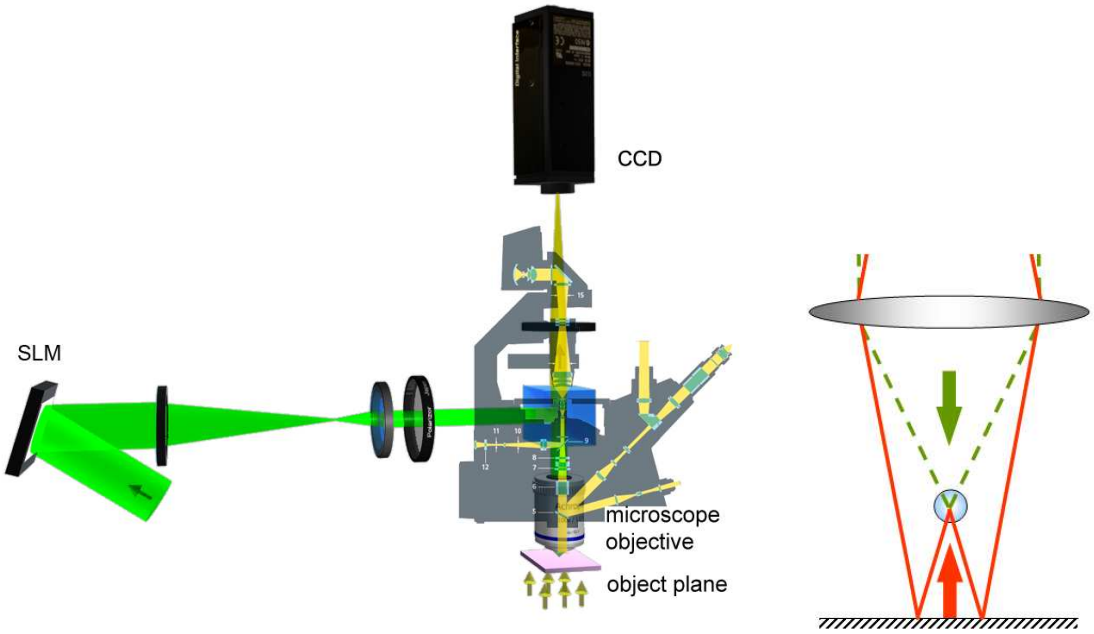

(a) Holographic Optical Tweezers (b) Twin Trap

Figure 1. Principle of the holographic optical tweezer setup and the twin trap: For every trap two light fields are holographically generated. The focus of the second trap lies – after reflection at the object slide – at the focus of the first trap.

Optical micro-manipulation as described above most often is realized by single-beam traps.[1] Therefore microscope objectives with high numerical aperture are employed in order to enable stable three-dimensional optical trapping. This is necessary in order to compensate the strong forward scattering force of single-beam traps. Aside from a comparatively simple realisation of such tweezers, there are some disadvantages like the very low depth of focus and the small working distances due to the necessary high numerical aperture. Also especially larger particles, which need higher intensity to be trapped may be damaged due to highly focused light.

To prevent these problems, so-called dual-beam traps can be used where two counter-propagating waves with low numerical aperture compensate the forward scattering forces of each other.[6–8] Such setups, which can e.g. be realized by well-aligned microscope objectives or fibers are unfortunately difficult to implement.

We propose a new dual-beam method which enables stable axial trapping with one single low numerical aperture microscope objective in a standard microscope. Holographic optical tweezers are used to generate two traps at different axial positions by holographically defocusing one of the traps. By reflecting one of the traps at a dichroitic object slide and bringing them to focus at the same point, a dual beam trap is realized (see Fig. 1(b)). The alignment of the counter-propagating spots is done by adapting the hologram.

Due to the coherence of the counter-propagating beams, a standing wave is generated in the spot of the twin trap. In real experiments with large particles the interference pattern is averaged out and no effect of the standing wave can be observed for the force. Therefore for our application with large particles in the range of 5 to 20 μm a ray optical model in principle is adequate to compute the trapping forces. For further details concerning the computation of the trapping forces see Zwick et al.[9]

Figure 2(a) shows the result of a ray optical simulation using non-sequential raytracing in Zemax and force computation in Matlab. The axial trapping force of a single trap (dashed line) as well as a twin trap (solid line) are shown for a water immersion microscope objective with NA=0.45. The force due to a single trap is asymmetric with a strong tendency to push the particle out of the trap (+z–direction), whereas the twin trap

features a symmetric trapping force as the scattering force is canceled. In this way the axial trapping force in the +z–direction is more then doubled (2.13 times compared to the single-beam trap).

Furthermore a detailed analysis concerning the tolerances of axial trap misalignment was done. Therefore one of the traps was shifted out of the common focus before being superimposed. In this way, a misalignment of the traps in + and − z direction was done. For the chosen setup and large particles an axial misalignment in the range of a few micrometers is tolerated (Fig. 2(b)).

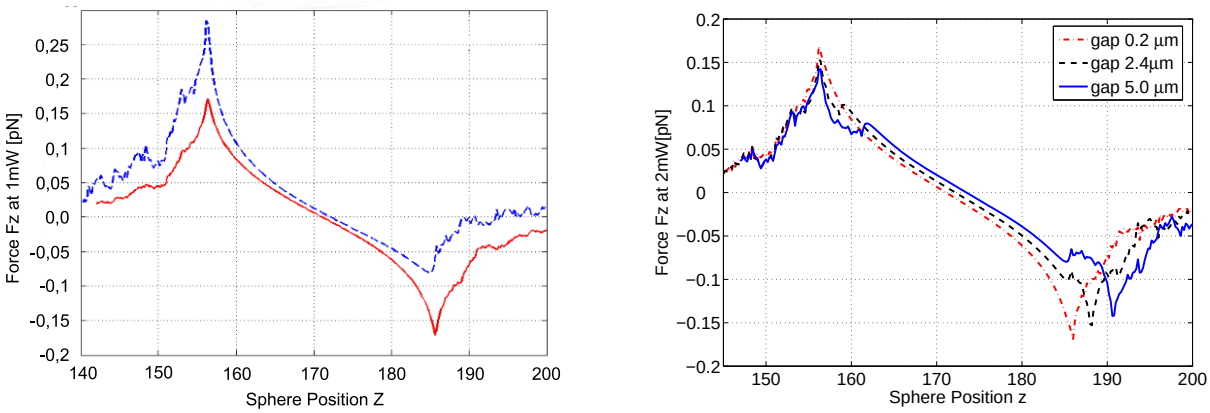

Figure 2. (a) Simulation of axial trapping force by non-sequential ray tracing of the trapping force for a single trap (dashed line) and a twin trap (solid line). The axial trapping efficiency is considerably improved in the forward (scattering) direction for the twin trap. (b) Simulation of axial trapping force of misaligned twin traps. The misalignment was $\pm 5\,\mu$m in z–direction for a $10\,\mu$m bead

In first experiments we were able to confirm the simulated results. Figure 3(a) shows a $3\,\mu$m polystyrene bead axially trapped by a twin trap. When turning off the reflected trap by changing the hologram, the bead is pushed out of the single-beam trap (Fig. 3(b)) towards the object slide due to the strong forward scattering force (Fig. 3(c)). In this experiment the distance between the twin trap and the reflecting object slide was approximately $25\,\mu$m.

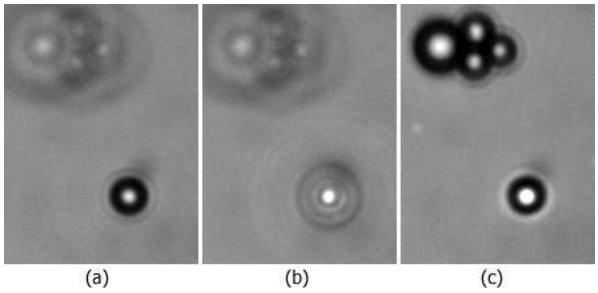

Figure 3. Stable axial trapping with a twin trap(a). By turning off the reflected trap, the bead is pushed out of the focus (b) toward the reflecting object slide (c).

2. HOLOGRAPHIC 4π-MICROSCOPY

Modern high-end light microscopy is capable of imaging below the diffraction limit by incorporating new fluorescence-based methods in combination with advanced numeric post-processing techniques. The most important techniques are confocal and structured illumination imaging, multi-photon microscopy, fluorescence microscopy with stimulated depletion, numeric deconvolution, apodization, and 4π-microscopy (see[10] for a good

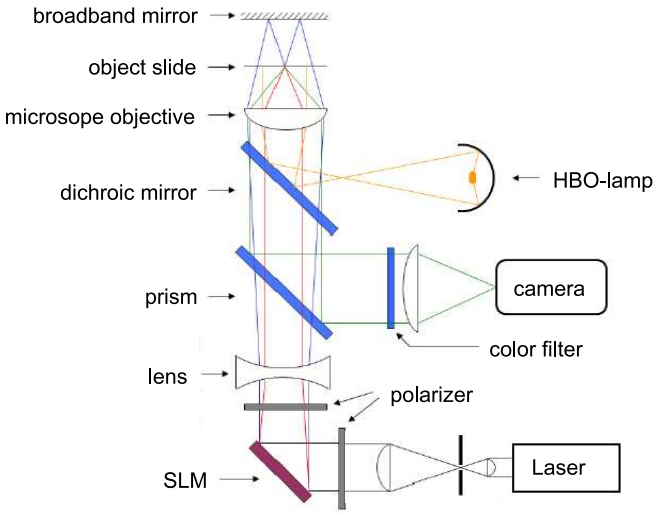

Figure 4. Setup used for holographic 4π experiments

overview). An especially interesting class of modern methods (4π-microscopy,[11] I5-microscopy,[12] standing wave microscopy,[13] interference confocal microscopy[14]) uses a focal region with a interference pattern of counter-propagating waves.

In a 4π setup, which conventionally is used together with fluorescence confocal imaging, the focal regions of two counter-propagating waves are coherently superimposed resulting in a considerably reduced central spot volume of the resulting 3D-point-spread function (PSF) and therefore an improved resolution. In practice a strong resolution enhancement is achieved in the axial direction and axial resolutions below 80 nm have been demonstrated.[15]

Depending on whether only illumination and/or detection is realized coherently from both sides one obtains slightly different imaging results and based on this difference in implementation typically a classification into type A, B, or C 4π-microscopy is done. 4π-microscopy can be (and has been) combined with a lot of other resolution enhancement techniques. Apart from multi-photon excitation, deconvolution, and pupil filters also stimulated emission depletion[16] has been employed.

Unfortunately up till now implementation of the method as well as its practical application is very complicated (two highly corrected microscope objectives, controlled by piezo stages and control of the environmental conditions) and therefore only one (expensive) commercial microscope is available. Kawata et al. proposed to simplify the setup by using a phase conjugating mirror (PCM) to generate the second, counter-propagating wave.[17] This has the additional advantage that aberrations of the counter-propagating wave automatically are canceled. Unfortunately the aberrations that would have been present in a conventional microscope (including aberrations due to the specimen) are still present and up till now the different possible realizations of the PCM also have their specific drawbacks (e.g. sensitivity, speed, reflectivity). Most significantly the sample has to be small so that the intensity of the counter-propagating beam is not strongly affected by the sample.

We propose a novel method of 4π-microscopy using a simple setup without mechanically moving parts by using the holographic double focus technique. One of the holographically generated foci is reflected by the object plate so that we obtain a 4π geometry with only one microscope objective and only one beam path (Fig. 4). This way conventional research microscopes could be used for 4π-microscopy.

The basic idea of an 4π-microscope is to use the standing wave that occurs due to the two coherent beams traveling in opposite directions. The interference maximum is used for the excitation of the fluorescence. To obtain the depth information the standing wave patterns is moved very precisely through the object. For a first step towards the implementation of a holographic 4π-microscope we will show that it is possible to holographically

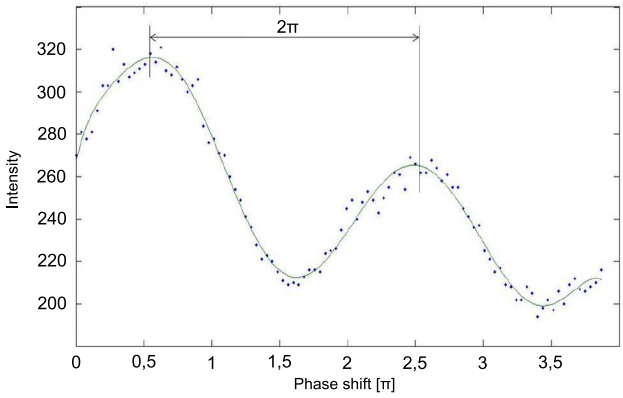

Figure 5. Recorded intensity for the holographically generated standing wave for the 4π experiments

generate the standing wave with only one microscope objective. Furthermore we will verify that we can move the standing wave very precisely along the optical path without any mechanical device just by modifying the hologram. The interference pattern due to the standing wave is exciting the fluorescent objects and for the method to work it is necessary that these fluorescent objects are smaller than half the pitch of the standing wave pattern. This is a major difference to the twin trap method discussed earlier, where the trapped particles are much larger than the standing wave pattern, which therefore effectively is averaged out.

Compared to the twin trap setup of section 1 we use a shorter wavelength laser (He-Ne laser Melles Griot 05-LLP-831, λ=632.8 nm, 5 mW). For the fluorescence we used the deep red fluorescent micro-spheres from PS-Speck. The micro-spheres have a diameter of 175 nm with an excitation wavelength of 633 nm and the emitted wavelength is 660 nm. We used an 50× objective with a numerical aperture of 0.7.

To reflect the upper focus back we used a broadband metallic mirror. To keep the holograms and the test as simple as possible we used the zeroth and first diffraction order for generation of the standing wave. A negative defocus term was employed in order to make the two beams focus at the same point in the object volume. To move the standing wave through the micro-sphere we shifted the phase of the hologram in small steps.

Figure 5 shows the vertical intensity gradient of the emitted light from the micro-sphere when shifting the phase of the hologram. One phase step was $1/25\,\pi$. For λ=633 nm this corresponds to 11 nm. The intensity of the second peak is smaller than the first peak due to the the bleaching of the micro-sphere. The distance between two peaks is 2π.

For a complete 4π imaging system the method should be automated so that a three-dimensional scanning by proper computation of the holograms is achieved. Parallelization is possible by using more complex holograms generating multiple double foci at the same time.

3. CHARACTERIZATION OF THE PHASE-MODULATING SLM

The phase modulation of the SLM used in the HOT system was characterized and optimized using two different experimental set-ups. First a fringe-shift measurement using a two-beam interference set-up was done. A laser beam is expanded and collimated and partially transmitted through a double-pinhole aperture. The two created coherent beams are incident onto dedicated areas of the microdisplay at a small incidence angle in order to separate incoming and outgoing beams. The beams are then spatially overlapped in order to create and detect interference fringes. This fringe pattern is spatially shifted as soon as the phase delay between the two partial beams changes.[18]

The phase modulation is dependent on the voltages applied to the LC cells of the microdisplay. These voltages are represented as pixels of graylevel images when the device is addressed using the graphics adapter of

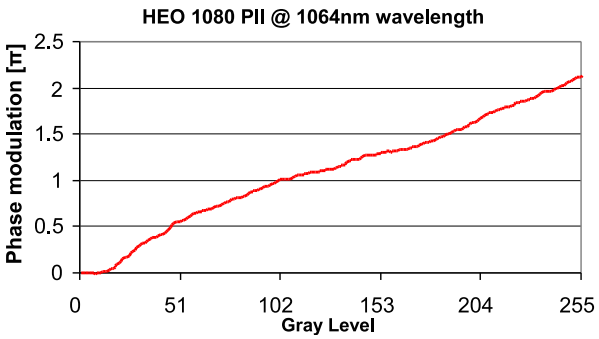

Figure 6. Phase modulation of a HEO 1080 P II spatial light modulator at 1064nm wavelength derived from a fringe-shift measurement

a computer, therefore the results shown in fig. 6 are given as a function of the addressed graylevel. The translation of a graylevel into a cell voltage is controlled by lookup tables (LUTs) stored in the electronic drive-board of the microdisplay. The curves shown have been obtained with tailored LUTs optimized for linear and full-2π range phase modulation of the device at 1064 nm, which is the wavelength of operation of the HOT system.

The phase modulation of a spatial light modulator can also be derived from the measurement of the diffraction at addressed binary linear gratings[19] (often referred to as Ronchi gratings). The curves in figure 7 show the measured intensity of two diffraction orders of a Ronchi grating with a grating constant of 1+1=2 pixels (1 pixel 'groove' and 1 pixel 'ridge'). For these measurements, images with one reference graylevel (usually 0 or 255) and one varying graylevel are used. As a result, phase gratings with variable phase modulation depth Φ are obtained, and the powers in the 0-th and $\pm$1-st diffraction orders are measured, permitting a derivation of the phase modulaton depth Φ.

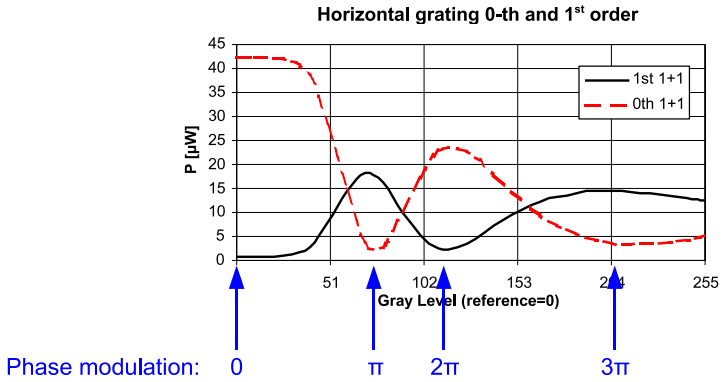

Figure 7. Power in the diffraction orders from a HEO 1080 P I spatial light modulator at 543 nm wavelength as a function of the graylevels, representing cell voltages and eventually a phase modulation depth.

Obviously, when the pixels representing the groove and the pixels representing the ridge of the grating are at the same graylevel, the SLM acts as a mere mirror and the power in the 1-st orders is zero. When the variable graylevel is changed, the 1-st orders gain power at the expense of the 0-th order until the phase delay is $\Phi = \pi$. When the difference between the graylevels is increased further, the power in the 1-st order is at a minimum for $\Phi = 2\pi$, at another maximum for $\Phi = 3\pi$ and so on.

The phase modulation that were obtained from the fringe-shift measurements and from the Ronchi diffraction measurement were in good agreement. For optimizing the device performance, the fringe-shift measurements seem to be preferable because for every combination of graylevels an exact phase shift can be determined, which eases the creation of LUTs for adjusting the phase reponse e. g. to a new wavelength of operation, while the

curves from the diffraction measurements would require a more sophisticated numerical fit procedure in order to deliver the values for such LUTs. However, the diffraction measurements provide additional information which cannot be obtained from the fringe-shift measurements.

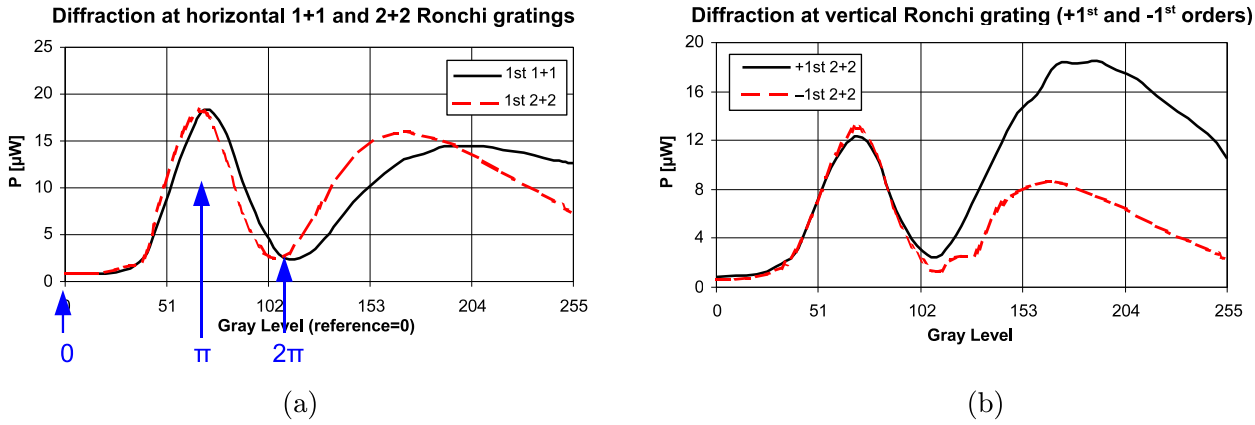

Figure 8. Diffraction orders from a HEO 1080 P I spatial light modulator at 543 nm wavelength for different grating constants (a) and diffraction directions (b)

The curves in figure 8(a) show that for smaller grating constants the graylevel (corresponding to the cell voltage) required for obtaining a certain phase shift is higher. This points to edge effects at the cell boundaries caused by fringe-field effects. The curves in figure 8(b) show an additional effect, as the diffraction efficiency in the ±1-st orders, which should be and for horizontal gratings indeed was found to be identical, is different for horizontal gratings especially for large cell voltages. Here the edge effects appear to introduce an asymmetrical phase modulation as a function of position, so that the grating in fact is not binary and instead has rounded shoulders and a certain blaze.

These derivations of the phase modulation from the ideal performance is especially observed for small grating constants, i. e. large spatial frequencies. In summary the SLM acts as a weak spatial-frequency low-pass with slight asymmetry in one spatial direction. Luckily, such effects can be compensated for by an inverse operation to the target signal which is eventually used for the hologram computations.

4. HOLOGRAM COMPUTATION ON THE GPU

For the optimization of more complicated holograms than the double foci we use the iterative Fourier transform algorithm (IFTA) with optimization areas and an user selectable normalization constant within the iteration loop. By this constant which is used to multiply the amplitude in the Fourier plane before copying the desired reconstruction into the reconstructed light field, one can chose if the optimization should favor diffraction efficiency or reconstruction quality.

After optimization it is possible to tile the holograms to the full SLM resolution in order to reduce speckle. The choice of the optimum hologram size is dependent on the application and the chosen (subjective or objective) rating of the reconstruction quality. Aberrations due to the overall system can be easily incorporated afterwards by subtracting the aberration from the optimized hologram.[20] Different methods are available for measuring the aberrations.[20, 21] Since the SLM is located in one plane, which is conjugate to the pupil of the system, up till now we only correct for aberrations in one isoplanatic patch.

Different approaches for accelerating the hologram computation have been employed in the past. Basically one can classify these approaches into three categories:

- Accelerated algorithms
- Fast special purpose hardware
- Fast general purpose hardware

Among the accelerated algorithms different approximation for computing the light field in the hologram plane for Fourier and Fresnel holograms,[22] the avoidance of redundant computation and look-up tables[23] as well as the use of symmetry have been proposed.[24] Also for display applications it is possible to use only horizontal parallax[25] which considerably speeds up computation. For special geometries like tilted reconstruction planes special formulas have been derived[26] and of course a large number of methods — mostly based on heuristics — have been proposed for improving the convergence of iterative optimization approaches or otherwise accelerating the computation.[27, 28]

Also specialized hardware have been used to improve the processing speed. Most prominent, the group of Lucente at the MIT used employed approaches (see e.g.[29]). Satake et al. used e.g. a 128 processor machine for the inverse problem, reconstructing digital holograms.[30] For hologram computation the FPGA-based HORN architectures are well known.[31]

Almost ten years ago people started to use graphics processing units (GPU) for the computation of holograms.[32] Since then the processing power of typical graphics units improved by a factor of more than 300 (given in triangles/second) for typical consumer hardware. Using the GPU became especially interesting during the last years because since then a standard GPU outperforms the central processing unit (CPU). The performance advantage is due to the strong parallelism (e.g. 128 floating point sub-processors in one GPU) that can be exploited for graphics programming as opposed to the less strong parallelism found in today's CPUs (e.g. quad-core CPUs).

It became soon obvious that this performance can be exploited for the computation of holograms.[32–34] In[36] we reported on an implementation of the iterative Fourier transform algorithm (IFTA) on a GPU. For this purpose we used the shading language "Cg". Since 2007 Nvidia made a new programming architecture, called "CUDA", available. Compared to the direct programming of the shaders via Cg or any other shader language, programming becomes more comfortable and already some optimized libraries, e.g. for performing fast Fourier transforms (FFT), are available.[35]

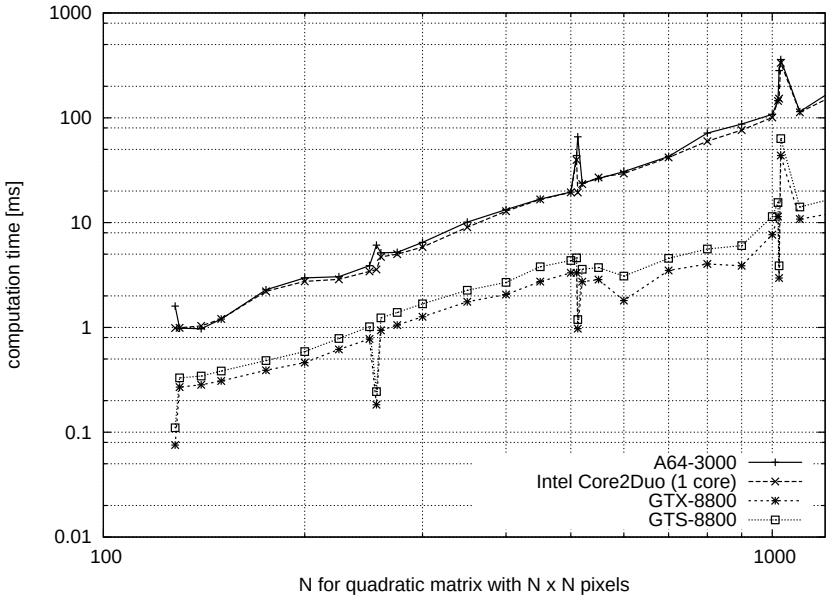

Figure 9. Benchmark for two-dimensional complex (32 bit accuracy) FFTs on different hardware platforms

We employed CUDA in order to implement IFTA-based hologram computations on Nvidia graphics boards of the 8800 series. Fig. 9 shows the results for performing two-dimensional complex (32 Bit accuracy) FFTs on a 8800-GTX and a 8800-GTS based card. Also the results for two different CPUs are shown. As can be seen we achieve a tremendous increase in performance. More than 1000 complex 2D-FFTs can be performed by one single 8800-GTX per second.

The main processing cost for each IFTA iteration in principle should be dominated by this FFT cost. Unfortunately we haven't yet achieved the full potentially available speed for IFTA. Up till now one IFTA loop at 512 x 512 pixel resolution takes 16.5 ms. Although this computational speed is much higher than that of our CPU-based solution (by a factor of about 10), our earlier Cg-based implementation[36] is still faster. However, we are working on the optimization on the CUDA-based solution to find the bottleneck which prevents to translate the gain in the FFT speed to a similar gain in speed of the whole IFTA and are confident that our efforts will be successful in the near future.

5. SUMMARY AND CONCLUSION

We have presented a HOT system at 1064 nm wavelength utilizing a holographic method for the generation of standing wave patterns with a standard research microscope. The method can be used for the trapping of particles with a single microscope objective with only low numerical aperture and for the implementation of 4π-microscopy. We also have shown results for the characterization of the employed HDTV-resolution LCoS SLM, in particular the fringe-field effects which are important for holograms including large spatial frequencies. Additionally we have shown that the hologram computation with iterative Fourier transform algorithms for our HOT system is faster using the GPUs of different NVidia graphics adapters than on the CPU. Currently the older Cg-based implementation is faster than the implementation based on the more recent CUDA programming architecture, but based on the remarkable speed increase of the CUDA-based FFT compared to the Cg-based FFT, we are sure that the CUDA-based hologram computation will soon be the fastest solution.

6. ACKNOWLEDGEMENTS

We thank the German Bundesministerium für Bildung und Forschung (BMBF, Aztek FKZ 13N8809) for financial support.

REFERENCES

1. A. Ashkin, J. M. Dziedzic, J. E. Bjorkholm, and S. Chu, "Observation of a single-beam gradient force optical trap for dielectric particles," *Opt. Lett.* **11**, 288 (1986).
2. Y. Hayasaki, S. Sumi, K. Mutoh, S. Suzuki, M. Itoh, T. Yataga, and N. Nishida, "Optical manipulation of microparticles using diffractive optical elements," *Proc. SPIE* **2778**, 229-230 (1996).
3. M. Reicherter, T. Haist, E. Wagemann, and H. J. Tiziani, "Optical particle trapping with computer-generated holograms written on a liquid-crystal display," *Opt. Lett.* **24**, 608 (1999).
4. T. Haist, S. Zwick, M. Warber, and W. Osten, "Spatial Light Modulators - Versatile Tools for Holography," *J. Holography Speckle* **3**, 125 (2006).
5. M. Reicherter, S. Zwick, T. Haist, C. Kohler, H. J. Tiziani, and W. Osten, "Fast digital hologram generation and adaptive force measurement in LCD based holographic tweezers," *Appl. Opt.* **45**, 888 (2006).
6. A. Ashkin, "Acceleration and Trapping of Particles by Radiation Pressure," *Phys. Rev. Lett.* **24**, 156 (1970).
7. A. Constable, J. Kim, J. Mervis, F. Zarinetchi, and M. Prentiss, "Demonstration of a fiber-optical light-force trap," *Opt. Lett.* **18**, 1867 (1993).
8. P. R. T. Jess, V. Garcés-Chávez, D. Smith, M. Mazilu, L. Paterson, A. Riches, C. S. Herrington, W. Sibbett, and K. Dholakia, "Dual beam fibre trap for Raman micro-spectroscopy of single cells," *Opt. Express* **14**, 5779 (2006).
9. S. Zwick, T. Haist, L. He, Y. Miyamoto, and W. Osten, "Holographic Twin Traps," *Optics Letters*, submitted
10. Y. Garini, B. J. Vermolen, I. T. Young, "From micro to nano: recent advances in high-resolution microscopy," Current Optinin in Microtechnology 16, 3-12 (2005)
11. S. Hell, and E.H.K. Stelzer, "Properties of a 4π confocal fluorescence microscope," *J. Opt. Soc. Am. A* 9, 2159 (1992)
12. M.G. Gustafsson, D.A. Agard, J.W. Sedat, "I5M: 3D widefield light microscopy with better than 100 nm axial resolution," *J. Microscopy* 195, 10-16. (1999)
13. B. Bailey, D. L. Farkas, D. L. Taylor, F. Lanni, "Enhancement of axial resolution in fluorescence microscopy by standing-wave excitation," *Nature* 366, 44 - 48 (1993)

14. C.J.R. Sheppard, and Y. Gong, "Improvement in axial resolution by interference confocal microscopy," *Optik* 87, 129-132 (1991)
15. J. Bewersdorf, A. Egner, S.W. Hell, "4π-microscopy," *Handbook of Biological Confocal Microscopy*, 3rd Edition (J. B. Pawley), Springer (2006)
16. M. Dyba, J. Keller, and S.W. Hell, "Phase filter enhanced STED-4π fluorescence microscopy: theory and experiment," *New Journal of Physics* 7, 1-21 (2005)
17. Y. Kawata, K. Fujita, O. Nakamura, and S. Kawata, "4π confocal optical system with phase conjugation," *Opt. Lett.* 21 , 1415-1417 (1996)
18. A. Hermerschmidt, S. Osten, S. Krüger and T. Blümel, "Wave front generation using a phase-only modulating liquid-crystal-based microdisplay with HDTV resolution", *Proc. SPIE* **6584**, 65840E (2007)
19. J. Oton, P. Ambs, M. S. Millan, and E. Parez-Cabra, "Multipoint phase calibration for improved compensation of inherent wavefront distortion in parallel aligned liquid crystal on silicon displays", *Appl. Opt.* **46**(23), pp. 5667-5679 (2007)
20. Reicherter, M., Gorski, W., Haist, T., Osten, W, "Dynamic correction of aberrations in microscopic imaging systems using an artificial point source," *Proc. SPIE* 5462, pp. 68-78 (2004)
21. J. Liang, B. Grimm, S. Goelz, J. F. Bille, "Objective measurement of wave aberrations of the human eye with use of a Hartmann-Shack wave-front sensor," J. Opt. Soc. Am. A 11, 1949-1957, (1994)
22. M. L. Tachiki, Y. Sando, M. Itoh, and T. Yatagai, "Fast calculation method for spherical computer-generated holograms," *Appl. Opt.* 45, 3527-3533 (2006)
23. J. L. Juárez-Pérez, A. Olivares-Pérez, and R. Berriel-Valdos, "Nonredundant calculation for creating digital Fresnel holograms," *Appl. Opt.* 36, 7437 (1997)
24. H. Eldeib, T. Yabe, T. Yoshino, "Efficient design of computer algorithm for improving the Gabor-type holography,", 'Computational Cybernetics and Simulation', 1997 IEEE International Conference on Systems, Man, and Cybernetics, vol. 4, pp.3148-3153 (1997)
25. V. M. Bove, Jr., W. J. Plesniak, T. Quentmeyer and J. Barabas "Real-Time Holographic Video Images with Commodity PC Hardware," *Proc. SPIE* 5664A (2005)
26. K. Matsushima, H. Schimmel, and F. Wyrowski, "Fast calculation method for optical diffraction on tilted planes by use of the angular spectrum of plane waves," *J. Opt. Soc. Am. A* 20, 1755-1762 (2003)
27. B. B. Chhetri, S. Yang, and T. Shimomura, "Stochastic Approach in the Efficient Design of the Direct-Binary-Search Algorithm for Hologram Synthesis," *Appl. Opt.* 39, 5956-5964 (2000)
28. J. -H. Li, K. J. Webb, G. J. Burke, D. A. White, and C. A. Thompson, "Design of near-field irregular diffractive optical elements by use of a multiresolution direct binary search method," *Opt. Lett.* 31, 1181-1183 (2006)
29. J. A. Watlington, M. Lucente, C. J. Sparrell, V. M. Bove, Jr., and I. Tamitani. "A hardware architecture for rapid generation of electro-holographic fringe patterns," *Proc. SPIE* 2406-23, 172-183 (1995)
30. S. Satake, H. Kanamori, T. Kunugi, K. Sato, T. Ito, and K. Yamamoto, "Parallel computing of a digital hologram and particle searching for microdigital-holographic particle-tracking velocimetry," *Appl. Opt.* 46, 538-543 (2007)
31. T. Ito, N. Masuda, K. Yoshimura, A. Shiraki, T. Shimobaba, and T. Sugie, "Special-purpose computer HORN-5 for a real-time electroholography," *Opt. Express* 13, 1923-1932 (2005)
32. A. Ritter, J. B¨ottger, O. Deussen, M. König, and T. Strothotte, "Hardware-based Rendering of Full-parallax Synthetic Holograms," *Appl. Opt.* 38, 1364-1369 (1999)
33. Haist, T., Reicherter, M.,Min Wu,Seifert L., "Using Graphics Boards to compute holograms," *Computing in Science & Engineering - January 2006*, pp. 8.-14 (2006)
34. Haist, T., Reicherter, M., Burla, A., Seifert, L., Hollis, M., Osten, W., "Fast hologram computation for holographic tweezers," *Proc. Fringe 2005*, pp. 126-133 (2005)
35. T. Haist, U. Schmid, W. Osten, "Fast computation of Fourier transforms by using graphics processing units," *VDI Berichte 1981* (ISBN 978-3-18-0901981-2), pp. 217-223 (2007)
36. Zwick, S., Warber, M., Haist, T., Osten, W., "Realisation of a holographic microlaser scalpel using a digital micro mirror device," *Proc. SPIE 6616N0* (2007)